



**HAL**  
open science

# Seismic internal stability of saturated reinforced soil retaining walls using the upper bound theorem of limit analysis

Hicham Alhajj Chehade, Daniel Dias, Marwan Sadek, Oriane Jenck, Fadi Hage Chehade

## ► To cite this version:

Hicham Alhajj Chehade, Daniel Dias, Marwan Sadek, Oriane Jenck, Fadi Hage Chehade. Seismic internal stability of saturated reinforced soil retaining walls using the upper bound theorem of limit analysis. *Soil Dynamics and Earthquake Engineering*, 2022, 155, pp.107180. 10.1016/j.soildyn.2022.107180 . hal-03929847

**HAL Id: hal-03929847**

**<https://hal.science/hal-03929847v1>**

Submitted on 22 Jul 2024

**HAL** is a multi-disciplinary open access archive for the deposit and dissemination of scientific research documents, whether they are published or not. The documents may come from teaching and research institutions in France or abroad, or from public or private research centers.

L'archive ouverte pluridisciplinaire **HAL**, est destinée au dépôt et à la diffusion de documents scientifiques de niveau recherche, publiés ou non, émanant des établissements d'enseignement et de recherche français ou étrangers, des laboratoires publics ou privés.



Distributed under a Creative Commons Attribution - NonCommercial 4.0 International License



26 **Consent to participate:** Not applicable  
27 **Consent for publication:** Not applicable  
28 **Availability of data and material:** Not applicable  
29 **Code availability:** Not applicable

30

## 31 **Acknowledgements**

32 The research team thanks the Lebanese University for partially funding this work.

33 **Abstract.** This study concerns the seismic internal stability analysis of saturated reinforced soil retaining walls using  
34 the discretization technique and the limit analysis upper bound approach. The discretization technique permits to  
35 generate the potential failure mechanism of reinforced structures point by point. The seismic forces are represented  
36 based on the pseudo-dynamic approach. This latter is more realistic than the pseudo-static one which is commonly used.  
37 It allows accounting for the dynamic characteristics of the seismic loading. Knowing that the water presence is the main  
38 cause of most failure cases reported in the literature, the pore water effect within the backfill soil is considered together  
39 with a possible crack opening in cohesive soils. The reinforcement strength required to prevent the saturated reinforced  
40 soil wall failure is obtained through an optimization process. The developed approach is validated by comparison with  
41 the existing results obtained by Abd and Utili (2017) using the conventional limit analysis method. The presence of  
42 pore-water pressure leads to an increase in the reinforcement strength required to prevent the failure. Discussions are  
43 then carried out to point out the effects of the crack presence, the seismic loading and the soil properties on the structure  
44 stability. The cases of non-homogeneous and layered soils are investigated.

45

46 **Keywords:** Reinforced soil, Pore water effect, Limit analysis, Discretization technique, Pseudo-dynamic approach.

## 47 **1 Introduction**

48 Geosynthetic reinforced soil retaining walls are now a mature technology. They are structures which allow  
49 reinforcing a compacted backfill with horizontal reinforcement elements connected to the wall facing. The  
50 reinforcements significantly improve the global shear strength. The success of these structures is mainly due to their  
51 advantages compared to conventional retaining walls, concerning cost, time and space saving, in addition to their good  
52 performance due to their flexibility during strong earthquakes.

53 A compacted cohesionless granular soil is recommended as a backfill in the reinforced zone by most design codes  
54 (e.g., FHWA, NF P 94-270). The use of a good drainage system is also required. These requirements avoid the

55 development of interstitial pore pressures in the reinforced zone. However, the use of geosynthetic reinforcements,  
56 which do not have corrosion risk that can affect the metallic reinforcements, gives the opportunity to use poorly  
57 draining cohesive soils when granular soils are not available or are expensive (Guler et al. 2007). This soil type was  
58 successfully used in the reinforced earth wall construction (Ricchio et al. 2014). Nevertheless, the use of these soils can  
59 lead to several problematical issues and therefore, reduce the system stability (Abd and Utili 2017). Among these  
60 problems, the pore-water pressures development and the crack formation in the backfill zone are the most dangerous  
61 ones. Koerner and Koerner (2018) presented 320 geosynthetic reinforced mechanically stabilized earth walls failure  
62 cases. They reported that the reinforced backfill soils used in 73% of these cases were cohesive ones. In addition, they  
63 reported that pore pressures developed in the reinforced backfill caused the failures of 63% of these walls.

64 The water presence in the cohesive backfill must be addressed due to its low permeability and the possible  
65 malfunction of the drainage system that could be caused by its clogging by fines. The system shear strength can then be  
66 significantly reduced. Furthermore, the cohesive soils present limited tensile strengths, and therefore, they can develop  
67 cracks on soil surface (Abd and Utili 2017). The cracks formation affects the reinforced cohesive soil retaining walls  
68 stability (Alhajj Chehade et al., 2019). This phenomenon has been observed at the surface of many reinforced cohesive  
69 slopes after earthquake events (Ling et al. 2001) in addition to the experimental studies (Porbaha and Goodings 1996).

70 The assessment of the seismic stability of reinforced soil structures could be performed using numerical approaches  
71 (finite differences-finite elements), limit equilibrium and limit analysis methods. The cracks introduce a discontinuity in  
72 the static and kinematic fields which induces a computationally-expensive cost to consider these discrete discontinuities  
73 in numerical methods (Utili and Abd 2016). Hence, to conduct a parametric study on the reinforced backfill retaining  
74 wall stability considering cracks formation, the use of numerical methods requires complex development. The most  
75 commonly used method to assess the unreinforced and reinforced slopes stability considering the cracks presence, in the  
76 literature, is the limit equilibrium one (Baker 1981; Chowdhury and Zhang 1991; Baker and Leshchinsky 2001, 2003).  
77 However, only the pre-existing crack case is considered through this method by the modification of the failure surface  
78 geometry. Alternatively, Chen et al. (1969) developed an efficient method to analyze slopes stability, known as the limit  
79 analysis method. Since then, this method has been used to assess the stability of all geotechnical structures including the  
80 reinforced soil walls. It permits to obtain more rigorous solutions considering the stress-strain relation of soils than the  
81 limit equilibrium does. In addition, it permits to include the process of crack propagation as a part of the failure  
82 mechanism. Recently, many studies assessed unreinforced slopes stability considering the cracks presence using the  
83 limit analysis upper bound approach (Michalowski 2013; Utili 2013; Zhao et al. 2016). In addition, Abd and Utili  
84 (2017) first investigated the effect of cracks on the stability of geosynthetic reinforced slopes. A homogeneous backfill  
85 soil was considered and two cracks types are examined, pre-existing cracks and cracks that can be formed as a part of  
86 the collapse mechanism.

87 In the reinforced soil wall stability analysis, a rotational toe log-spiral failure surface is generally considered as the  
88 most critical failure mechanism (Abd and Utili 2017; Alhaji Chehade et al. 2019, 2020). Mollon et al. (2011) developed  
89 a discretization method coupled with the kinematic approach of limit analysis, in the framework of face stability  
90 assessment of circular tunnels. The discretization technique permits to overcome the conventional kinematic approach  
91 limitations by generating the failure mechanism point by point. It allows the consideration of non-uniform soils and the  
92 use of the pseudo-dynamic approach to represent the seismic loading instead of the pseudo-static one, which is more  
93 realistic. The good agreement of the results with the field measurements in the work of Mollon et al. (2011), inspired  
94 many researchers to extend the discretization-based kinematic analysis to assess the stability of different geotechnical  
95 structures (Pan and Dias 2015; Qin and Chian 2018; Sun et al. 2018). In this context, Alhaji Chehade et al. (2019)  
96 successfully extended it to generate a toe log-spiral failure mechanism in the framework of reinforced soil walls  
97 stability assessment.

98 In this study, the limit analysis upper bound theorem is employed for the seismic stability assessment of  
99 geosynthetic reinforced soil retaining walls with saturated non-uniform backfill soils. A rotational failure mechanism  
100 generated point by point through the discretization technique is considered. This technique gives the possibility to  
101 represent the seismic loading through the pseudo-dynamic approach as well as the possibility of considering non-  
102 homogeneous backfill soil. A saturated cohesive backfill soil is considered. The influences of the pore water pressure,  
103 the cracks presence, the soil heterogeneity and the seismic loading on the seismic internal stability of reinforced soil  
104 retaining walls are assessed and discussed.

## 105 **2 Upper bound theorem of limit analysis**

106 The upper bound theorem of limit analysis is based on the balance between the internal and external forces of a  
107 kinematically admissible velocity field. An advantage of this method is the consideration of the soil stress-strain  
108 relationship through the concept of yield criterion and its associated flow rule. Nevertheless, among the disadvantages of  
109 this method is that the shape of the failure surface is imposed. In addition, the soil behavior is assumed to be an ideal  
110 rigid, perfectly plastic body with an associated normality rule based on the Coulomb yield condition, which is not  
111 rational.

112 In this study, the kinematic theorem is applied to analyze the seismic internal stability of geosynthetic reinforced  
113 soil retaining walls in saturated poorly draining backfills. A rigid block assumption is considered and the soil is  
114 considered as an ideal rigid perfectly plastic material obeying associated flow rule. This theorem gives a rigorous lower  
115 bound to the required reinforcement tensile strength that prevents the failure of the reinforced soil walls. The reinforced  
116 wall fails if the external work rate exceeds the internal energy dissipation rate for any assumed kinematically admissible  
117 failure mechanism. A rotational log-spiral failure mechanism passing through the wall toe is assumed (Abd and Utili

118 2017; Alhadj Chehade et al. 2019a, 2020). The geosynthetic reinforcements only resist tension without any bending or  
119 compression resistance. These reinforcements are finite in number, having a uniform length, placed with a uniform  
120 vertical spacing, providing therefore a uniform tensile strength distribution over depth. They are placed horizontally and  
121 provide forces that correspond to their tensile strength or pullout resistance.

### 122 3 Discretization technique

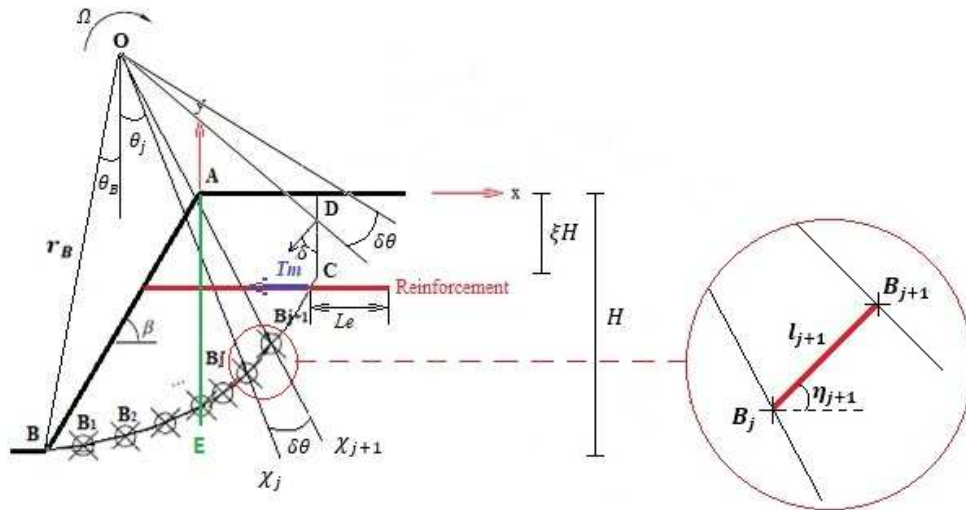
123 The discretization technique was proposed for the first time by Mollon et al. (2011) to generate a rotational failure  
124 mechanism, in the framework of the stability analysis of circular tunnels. Alhadj Chehade et al. (2019) extended this  
125 technique for reinforced soil retaining walls stability assessment. It allows to overcome the limitations of the traditional  
126 kinematic approach which can only be used in case of homogeneous soils and can only represents the seismic loading  
127 by the pseudo-static approach (Alhadj Chehade et al., 2019). This is because when the sliding surface is generated point-  
128 by-point through this technique, the soil properties and the seismic loading could be easily specified for each  
129 infinitesimal part of the failure surface. In this paper, a log-spiral failure mechanism passing by the wall toe is generated  
130 using this technique as illustrated in Fig. 1. A level backfill is considered (Horizontal surface),  $H$  denotes the wall  
131 height and  $\beta$  is the angle formed between the horizontal and the wall facing.

132 The failure surface  $ABCD$  delimits the moving soil area and the soil at rest. It is formed by the log-spiral surface  $BC$   
133 and the potential formed crack  $CD$ . Along the first surface, the soil fails purely in shear while it can also fail in tension  
134 along the crack. The failure surface is defined by the parameters  $r_B$ ,  $\theta_B$  and  $\xi$ .  $r_B$  corresponds to the length of  $OB$ ,  $\theta_B$   
135 corresponds to the angle between the vertical direction and the  $(OB)$  and  $\xi$  is the ratio of the crack depth to the wall  
136 height. Two cracks' cases can be involved in the failure mechanism. Pre-existing cracks in the reinforced soil due to  
137 weathering, desiccation and other climate phenomenon, and cracks that are formed during the collapse mechanism  
138 process. For simplicity in this study and similar to various studies (Michalowski 2013; Utili 2013; Zhao et al. 2016), the  
139 cracks considered are assumed to be vertical even though they can presented curved shapes as reported by Hu et al.  
140 (2010). For rigid blocks assumption, the soil block  $ABCD$  is rotating about the center  $O$  with an angular velocity  $\Omega$ . The  
141 center of rotation  $O$  can be defined by the mechanism parameters  $r_B$  and  $\theta_B$ . The discretization technique aims at  
142 defining the failure surface by a series of points  $B_j$  iteratively i.e. each point is derived from the previous point,  
143 knowing that the wall toe is the starting point of the generation process. The normality condition should be respected in  
144 order to obtain a kinematically admissible failure mechanism. Therefore, the angle between each segment  $[B_j B_{j+1}]$   
145 formed by two consecutive points on the failure surface, and the velocity vector should be equal to the soil friction  
146 angle  $\varphi_i$ . This angle becomes equal to  $\delta$  along the vertical crack  $CD$  as depicted in Fig.2. The angle  $\delta\theta$ , known as the  
147 discretization angle, denotes the angle between two consecutives radial lines,  $\chi_j$  and  $\chi_{j+1}$ . The accuracy of the failure

148 mechanism is affected by this angle. A closer match to the log-spiral failure mechanism is obtained with small values of  
 149 this angle. The detailed steps and equations used to generate the failure mechanism are presented in (Alhajj Chehade et  
 150 al., 2019).

151

152



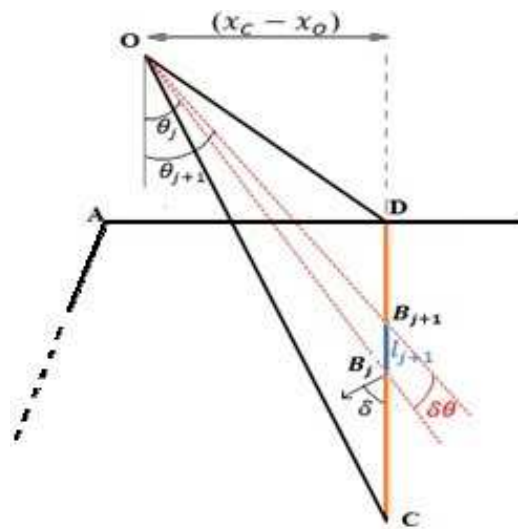
153

154

Fig.1. Generation of the potential failure surface by the discretization technique

155

156



157

158

159

Fig.2. Generation of the crack

#### 160 4 Pseudo-dynamic approach

161 The use of the real-time acceleration history to represent a seismic event is always the best choice. Such approach  
 162 requires a high computational effort using numerical analysis. However, the seismic loading is commonly represented

163 using the pseudo-static approach when the former approach is not justifiable. In the framework of this approach, the  
 164 seismic accelerations are considered constants. Alternatively, Steedman and Zeng (1990) proposed a more realistic  
 165 approach, the pseudo-dynamic one, to represent the seismic loading through the limit equilibrium method. It represents  
 166 a good compromise between the pseudo-static accelerations and the real-time acceleration history. It accounts for the  
 167 time and spatial variation of the seismic shaking. The discretization method allows the use of this approach with the  
 168 kinematic theorem of limit analysis to represent the seismic loading which is not applicable in case of conventional  
 169 limit analysis method (Qin and Chian 2017, 2019).

170 The pseudo-dynamic analysis considers finite shear and primary wave velocities acting within soil medium, while  
 171 the pseudo-static one assumes infinite values. The soil shear modulus  $G$  is assumed to remain constant during the  
 172 shaking in the whole soil medium. This means that the shear wave velocity  $V_s$  and the primary wave velocity  $V_p$  that  
 173 depend on  $G$ , remain also constant. On the other hand, the accelerations magnitudes and phases vary in both directions  
 174 along the backfill depth. The ratio  $V_p/V_s = 1.87$ , used for soils characterized with a Poisson's ratio  $\nu = 0.3$ , is  
 175 considered in this paper.

176 In reality, as mentioned before, the real time history acceleration with a wide frequency content is the best way to  
 177 consider an earthquake. For simplicity, similar to most previous studies (Choudhury and Nimbalkar, 2006; Nimbalkar  
 178 et al. 2006; Ahmad and Choudhury 2008; Basha and Sivakumar Babu 2011; Qin and Chian 2017, 2019; Alhadjj Chehade  
 179 et al. 2019a, 2020), this work adopt a sinusoidal acceleration. The accelerations magnitudes in both directions are  
 180 assumed to vary linearly along the reinforced backfill depth. If the accelerations are amplified by a factor  $f$  at the  
 181 ground surface related to the accelerations at the wall base, the horizontal and vertical acceleration expressions at any  
 182 depth  $y$  and time  $t$  can be expressed as:

$$183 \quad \begin{cases} a_h = \left[ f + \frac{y}{H}(f - 1) \right] \cdot k_h g \sin \frac{2\pi}{T} \left( t - \frac{H + y}{V_s} \right) \\ a_v = \left[ f + \frac{y}{H}(f - 1) \right] \cdot k_v g \sin \frac{2\pi}{T} \left( t - \frac{H + y}{V_p} \right) \end{cases} \quad (1)$$

184 where  $H$  is the wall height,  $g$  the acceleration due to gravity,  $T$  the lateral and vertical shakings period,  $k_h$  and  $k_v$  the  
 185 horizontal and vertical seismic coefficients respectively.

## 186 **5 Discretization-based kinematic analysis**

187 The limit analysis kinematic approach is based on the balance between internal energy dissipation  $\dot{D}$ , and the work  
 188 rates of the external forces,  $\dot{W}$ , in any kinematically admissible failure mechanism. Its application gives a lower bound  
 189 to the required tensile reinforcement strength  $T_m$ , which ensures the reinforced soil wall stability.



190 The internal energy dissipation during the failure process takes place in the geosynthetic reinforcing elements by  
 191 tensile failure or/and along the reinforcing elements by pullout failure. In addition, based on the rigid blocks  
 192 assumption, an internal energy is dissipated along the discontinuity surface due to the soil plastic deformation. When  
 193 the failure mechanism involves the cracks presence, the internal energy dissipation along the crack  $CD$  must be  
 194 accounted only in the case of crack that forms during the failure mechanism process since an amount of energy is  
 195 required for its formation (Michalowski, 2013). On the other hand, for a pre-existing crack that is already present in the  
 196 soil,  $\dot{D}_{CD}=0$ .

197 On the other hand, the external work rates involve the soil block weight  $ABCD$  work rate, the inertia forces work  
 198 rates representing the seismic loading in both directions and the pore water pressure one.

199 The required tensile reinforcement strength to maintain the reinforced soil wall equilibrium, can be determined by  
 200 equating the external work rates and the internal energy dissipations, as stated by the kinematic theorem of limit  
 201 analysis. This approach provides a lower bound for the required strength through an optimization procedure. The  
 202 energy balance equation is given by:

$$203 \quad \dot{W}_\gamma + \dot{W}_{kh} + \dot{W}_{kv} + \dot{W}_u = \dot{D}_{BC} + \dot{D}_{CD} + \dot{D}_T \quad (2)$$

204 Where  $\dot{W}_\gamma$  is the soil weight work rate ;  $\dot{W}_{kh}$  and  $\dot{W}_{kv}$  are the seismic forces work rates ;  $\dot{W}_u$  is the pore-water pressure  
 205 work rate;  $\dot{D}_{BC}$ ,  $\dot{D}_{CD}$  and  $\dot{D}_T$  are the internal energy dissipated along the rotational part of the sliding surface, along the  
 206 vertical crack and, in and along the reinforcements respectively.

207 Due to the discretization, the computations of the external work rates are performed by summation of the elementary  
 208 work rates of the elementary trapezoidal surface  $B'_j B_j B'_{j+1} B_{j+1}$  shown in Fig. 3 and are expressed as:

$$209 \quad \dot{W}_\gamma = \sum_j (\gamma \cdot A_j) \cdot (\Omega \cdot (x_{Gj} - x_o)) \quad (3)$$

$$210 \quad \dot{W}_{kh} = \sum_j \left( \gamma \cdot A_j \cdot \left[ f + \frac{y_{Gj}}{H} (f - 1) \right] \cdot k_h \sin \frac{2\pi}{T} \left( t - \frac{H + y_{Gj}}{V_s} \right) \right) \cdot (\Omega \cdot (y_o - y_{Gj})) \quad (4)$$

$$211 \quad \dot{W}_{kv} = \sum_j \left( \gamma \cdot A_j \cdot \left[ f + \frac{y_{Gj}}{H} (f - 1) \right] \cdot k_v \sin \frac{2\pi}{T} \left( t - \frac{H + y_{Gj}}{V_p} \right) \right) \cdot (\Omega \cdot (x_{Gj} - x_o)) \quad (5)$$

212  
 213  
 214 where  $A_j$  is the infinitesimal area of the trapezoidal element  $B'_j B_j B'_{j+1} B_{j+1}$ ;  $x_{Gj}$  and  $y_{Gj}$  are the coordinates of its  
 215 gravity center  $G_i$ ;  $x_o$  and  $y_o$  are the center of rotation coordinates of the rotational failure mechanism  $O$ .  
 216



241 The first term in Eq. (7) is assumed to be zero since a rigid block is considered. In the framework of the failure  
 242 surface generation using the point-to-point method, the kinematical admissibility condition must be satisfied and  
 243 therefore, the velocity vector must be inclined by to the failure surface by an angle equal the soil friction angle  $\varphi$ .  
 244 Hence the angle between the vector  $n_i$  and the velocity vector is equal to  $\frac{\pi}{2} + \varphi$ . The velocity vector of the collapse  
 245 block at a point  $B_j$  of the failure surface is equal to the product of the angular velocity  $\Omega$  by the length of  $[OB_j]$ ,  $L_j$ . The  
 246 pore-water pressure work rate along the failure surface is then given by the summation of elementary work rates as  
 247 follows:

$$248 \quad \begin{cases} \dot{W}_u = \sum_j r_u \cdot \gamma \cdot (x_j \cdot \tan \beta - y_j) \cdot l_j \cdot \Omega \cdot L_j \cdot \sin \varphi & \text{along the boundary surface } BE \\ \dot{W}_u = \sum_j r_u \cdot \gamma \cdot (-y_j) \cdot l_j \cdot \Omega \cdot L_j \cdot \sin \varphi & \text{along the boundary surface } ED \end{cases} \quad (8)$$

249 where  $x_j$  and  $y_j$  are the coordinates of point  $B_j$  and  $l_j$  is the length of  $[B_{j-1}B_j]$ .

250 Since rigid blocks assumption is considered, the internal energy dissipation occurs along the sliding surface that  
 251 separates the failure region and the soil at rest, and along the reinforcements. The internal energy dissipated along the  
 252 sliding surface is divided into two parts: along the log-spiral part and along the vertical crack. Eq. 9 gives the  
 253 expression of  $\dot{D}_{BC}$ , as a summation of the internal work rate per infinitesimal length as follows:

$$254 \quad \dot{D}_{BC} = \sum (c_j \cdot (L_j \cdot \Omega \cdot \cos \varphi_j) \cdot l_j) \quad (9)$$

255 Where  $L_j$  and  $l_j$  are respectively the lengths of the segments  $[OB_j]$  and  $[B_{j-1}B_j]$ ,  $c_j$  and  $\varphi_j$  are respectively the soil  
 256 cohesion and the soil friction angle at the point  $B_j$ .

257 Eq. 10 gives the internal energy dissipation along the vertical crack  $CD$  for soil tensile cut-off (zero tensile strength)  
 258 which is generally assumed for safety reasons. On the other hand, Eq. 11 gives the energy dissipated in the  
 259 reinforcement  $\dot{D}_T$  due to its tensile failure.

$$260 \quad \begin{cases} \dot{D}_{CD} = \sum c_j \Omega L_j \cos \varphi_j \frac{1 - \sin \delta_j}{1 - \sin \varphi_j} l_j & \text{Crack formation (tension cut - off)} \\ \dot{D}_{CD} = 0 & \text{Pre - existing crack} \end{cases} \quad (10)$$

261

262

$$263 \quad \begin{cases} \dot{D}_T = \sum \left( \frac{n_r T_t}{H} \cdot l_j \cdot \sin \eta_j \cdot \Omega \cdot L_j \cdot \cos(\theta_B + j \cdot \delta \theta) \right) & \text{along the boundary BC} \\ \dot{D}_T = \sum \left( \frac{n_r T_t}{H} \cdot l_j \cdot \Omega \cdot L_j \cdot \cos(\theta_B + j \cdot \delta \theta) \right) & \text{along the vertical crack CD} \end{cases} \quad (11)$$

264

265 where  $\eta_j$  is the angle that forms  $[B_{j-1}B_j]$  with the horizontal axis,  $\delta_j$  is the angle between the vertical crack  $CD$  and the  
 266 velocity vector,  $T_t$  is the reinforcement tensile strength and  $n_r$  is the reinforcement layers number.

267 In most previous studies, the required reinforcement strength is calculated considering only this reinforcement  
 268 failure type. Concerning the reinforcement length, it is determined through an optimization process in a such a way that  
 269 when considering the combined failure mode (rupture in some reinforcement layers and pullout in the others), the  
 270 required reinforcement strength remains the same as obtained previously when considering only the tensile failure  
 271 mode. However, this method can lead to unpractical reinforcement lengths in many cases. Alhadj Chehade et al. (2019,  
 272 2020) consider for the first time the combined reinforcement failures modes (tensile and pullout failures)  
 273 simultaneously, with a pre-fixed reinforcement length. The internal energy dissipated along a single reinforcement due  
 274 to pullout failure mode, is expressed as:

$$275 \quad d\dot{D}_p = T_p \Omega Y_i \quad (12)$$

276 where  $T_p$  is the pullout resistance of the considered reinforcement layer,  $Y_i$  is the vertical distance between the  
 277 geosynthetic layer and the rotation center  $O$ .

278 Note that the pullout force calculation for the internal energy dissipation along the reinforcements, should account  
 279 for the water presence. It can then be written as:

$$280 \quad T_p = 2\gamma z^*(1 - r_u)L_e f^* \quad (13)$$

281 where  $z^*$  is the overburden depth;  $L_e$  is the length of the reinforcement beyond the failure surface, known as the  
 282 effective length;  $f^*$  is the apparent friction coefficient at the soil/reinforcement interface.

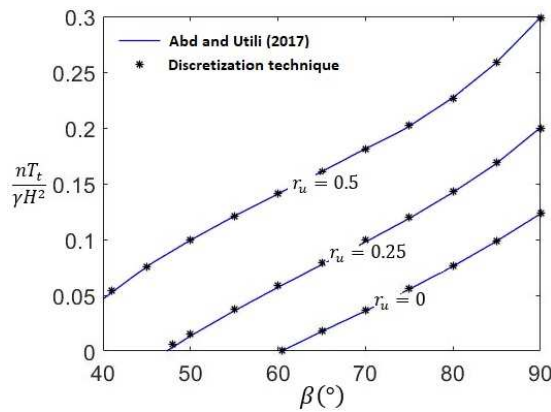
283 A lower bound to the required reinforcement is determined using a two-step genetic algorithm proposed by Guo et  
 284 al. (2018) to perform an optimization process with respect to four variables, namely  $[r_B, \theta_B, \xi, t]$ . The length of  $[OB]$ ,  
 285  $r_B$ , the angle between  $(OB)$  and the vertical direction,  $\theta_B$ , and the normalized crack depth,  $\xi$ , are the geometrical  
 286 parameters that define the failure surface (Fig.1a), while  $t$  is the time involved in the pseudo-dynamic approach. The  
 287 interested readers are referred to Guo et al. (2018) for detailed description of the two-step genetic algorithm.

## 288 **6 Comparison with the existing solutions**

289 In order to validate the robustness of the proposed discretization mechanism, the obtained results are compared with  
 290 those by Abd and Utili (2017) obtained using the conventional limit analysis method. Abd and Utili (2017) used the  
 291 conventional upper bound approach of limit analysis in order to evaluate the reinforcement strength required to ensure  
 292 the internal stability of geosynthetic reinforced slopes under static conditions. The effect of pre-existing crack is  
 293 investigated. Only the reinforcement tensile failure is considered to determine the reinforcement strength while the

294 reinforcement length is calculated in such a way that the required reinforcement strength do not need to be increased  
 295 when considering reinforcement tensile and pullout failures. They assumed both linear (uniform) and triangular  
 296 reinforcement distribution. The pore water pressure effect on the required reinforcement tensile strength was analyzed  
 297 by considering the same approach used here through the so-called pore-water pressure coefficient  $r_u$ .

298 In order to validate the application of the discretization method in this study, the results of the discrete method are  
 299 obtained under the same conditions used in the work of Abd and Utili (2017). The case of the crack that is formed as a  
 300 part of the failure mechanism is considered. The soil is considered without tensile strength (tension cut-off). The  
 301 comparisons of results are depicted in Fig. 4. for different walls inclinations  $\beta$ , and coefficients  $r_u$ . The good agreement  
 302 between the two methods shows the efficiency of the proposed method.



303  
 304 **Fig. 4.** Comparison of the conventional limit analysis and the discretization technique ( $\varphi = 20^\circ$  and  $c/\gamma H = 0.1$ )

305 **7 Numerical results**

306 *7.1 Required reinforcement strength for reinforced homogeneous soil retaining wall*

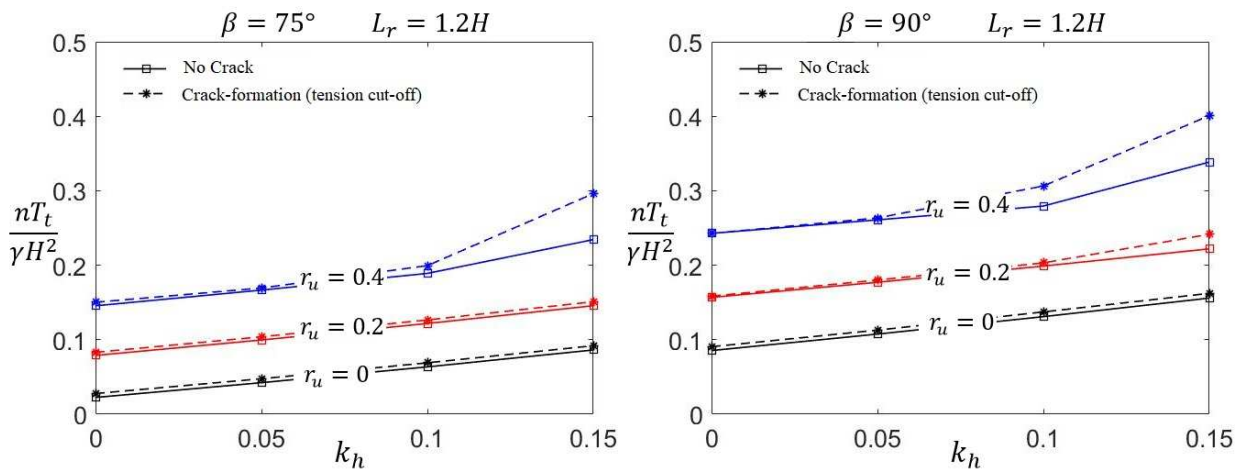
307 To investigate the pore-water pressure effect, tension crack and seismic loading, the results in terms of required  
 308 reinforcement strength in a normalized form are presented for two wall inclinations  $\beta = 75^\circ$  and  $\beta = 90^\circ$ . The two  
 309 reinforcement failures modes are considered simultaneously. The following parameters are considered:  $H=7\text{ m}$ ,  
 310  $\gamma=18\text{ kN/m}^3$ ,  $\varphi=25^\circ$ ,  $c=12.6\text{ kPa}$ ,  $\lambda=0.5$ ,  $L_r=1.2\text{ H}$ ,  $n_r=10$ ,  $f_0^*=1.2$ ,  $f_1^*=0.6$ ,  $f=1.2$ ,  $V_s=150\text{ m/s}$ ,  $V_p=280.5\text{ m/s}$ ,  
 311 and  $T=0.3\text{ s}$ , where  $\lambda=k_v/k_h$ ,  $c$  the soil cohesion,  $L_r$  the reinforcement length,  $n$  the reinforcement number,  $f_0^*$  and  $f_1^*$   
 312 are the initial and the minimum apparent friction coefficients at the soil/strip interface.. The discretization angle  $\delta\theta$  is  
 313 considered to be equal to  $0.01^\circ$  in this paper, since this value represents a good compromise between accuracy and time  
 314 calculation according to Alhajj Chehade et al. (2021).

315 According to fig. 5, it is observed that the required reinforcement strength increases with the horizontal seismic  
 316 coefficient, the pore-water ratio and the wall inclination ( $\beta$ ). Considering the crack formation as a part of the failure

317 mechanism leads to larger required reinforcement strength values than the ones obtained when considering an intact  
 318 soil.

319 It is evident that increasing the horizontal seismic coefficient  $k_h$ , increases the required reinforcement tensile  
 320 strength. Moreover, the pore-water pressure is found to be unfavorable to the reinforced soil wall stability. The presence  
 321 of cracks leads to larger required reinforcement strength. In particular, when the value of the pore-water pressure or of  
 322 the seismic loading is important, the required reinforcement strength increase is more obvious. Hence, it is critical to  
 323 consider these effects when poorly draining cohesive soils are used, as backfill materials, in seismic zones for economic  
 324 reasons.

325



326

327

**Fig. 5.** Required reinforcement strength against seismic coefficient for intact and cracked backfills

328 The reinforcement strength required to prevent the failure of geosynthetic reinforced soil retaining wall, for different  
 329 values of horizontal seismic coefficient, pore-water ratio and wall inclination ( $\beta$ ) are also presented in Table1. Two  
 330 crack cases are considered. Table 1 presented also the normalized crack depth  $\xi$  in case of crack formation as a part of  
 331 the failure mechanism. The results showed that the normalized crack depth  $\xi$  of the critical failure surface generally  
 332 decreased with the increase of  $\beta$  and  $k_h$ . However, when the pore-water ratio is high ( $r_u = 0.4$ ), some exceptions  
 333 observed.

334

**Table 1** Required reinforcement strength and normalized crack depth for different values of  $r_u$  and  $k_h$ .

$r_u$	$k_h$		$\frac{nT_t}{\gamma H^2}$		Normalized crack depth $\xi$	
			$\beta = 75^\circ$	$\beta = 90^\circ$	$\beta = 75^\circ$	$\beta = 90^\circ$
0	0	No crack	0.025	0.085	-	-
		Crack formation	0.028	0.091	0.241	0.222

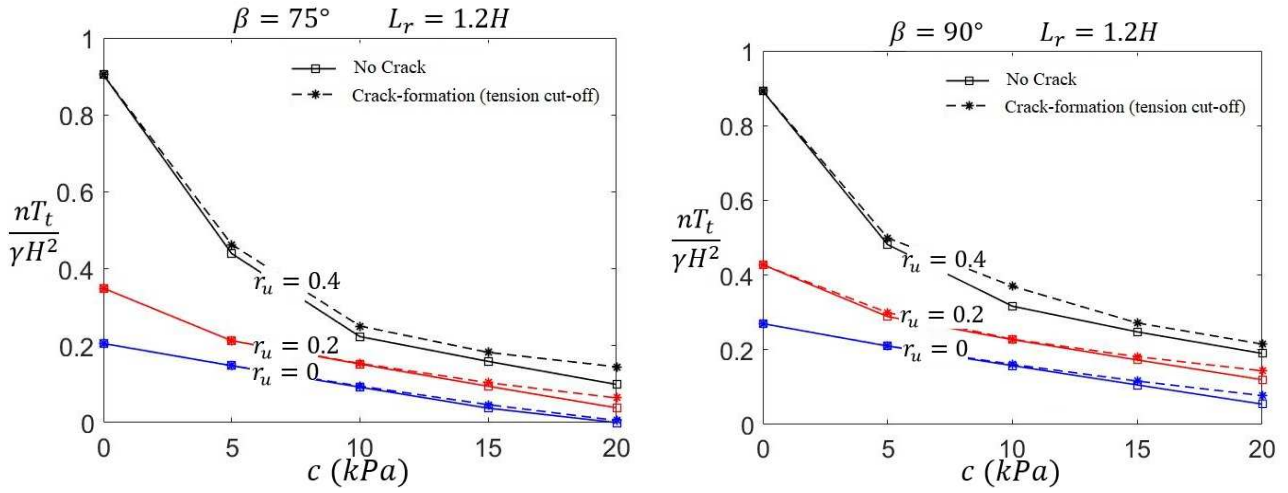
0.05	No crack	0.042	0.108	-	-
	Crack formation	0.048	0.113	0.220	0.207
0.1	No crack	0.064	0.131	-	-
	Crack formation	0.069	0.137	0.204	0.196
0.15	No crack	0.086	0.156	-	-
	Crack formation	0.092	0.162	0.190	0.187
0.2	No crack	0.079	0.157	-	-
	Crack formation	0.083	0.159	0.321	0.277
0.05	No crack	0.100	0.177	-	-
	Crack formation	0.104	0.180	0.282	0.252
0.1	No crack	0.122	0.199	-	-
	Crack formation	0.127	0.203	0.254	0.232
0.15	No crack	0.146	0.222	-	-
	Crack formation	0.151	0.242	0.230	0.164
0.4	No crack	0.146	0.243	-	-
	Crack formation	0.150	0.243	0.597	0
0.05	No crack	0.167	0.261	-	-
	Crack formation	0.169	0.263	0.466	0.003
0.1	No crack	0.189	0.279	-	-
	Crack formation	0.199	0.306	0.318	0.350
0.15	No crack	0.234	0.339	-	-
	Crack formation	0.296	0.401	0.510	0.450

335

336 Fig.6 shows the soil cohesion effect on the reinforcement strength required to prevent the reinforced soil wall  
337 failure, considering different pore-water coefficients values for a homogeneous backfill soil. The horizontal seismic  
338 coefficient is equal to 0.1. The pore pressure coefficient increase leads to a significantly increase of the normalized  
339 reinforcement strength. It is clear that the soil cohesion improves wall stability. When the soil cohesion increases, the  
340 normalized required reinforcement strength decreases for different values of  $r_u$ , for both reinforced earth walls  
341 inclinations. The influence of the soil cohesion is more pronounced in the case of a pore-water coefficient  $r_u$  equal to  
342 0.4. The required reinforcement strength is slightly greater for the crack presence case. The discrepancy between the  
343 curves corresponding to the cases of crack formation and no crack is more noticeable when the soil cohesion increases.

344 For the inclined retaining wall with  $\beta = 75^\circ$ , for a soil cohesion  $c$  higher than  $19 \text{ kPa}$  and a pore-water coefficient  
345  $r_u$  equal to zero, the required reinforcement strength which ensure the reinforced soil wall stability is zero. There is no  
346 need to reinforced the backfill area with geosynthetic elements.

347



348

349

**Fig. 6.** Required reinforcement strength against soil cohesion for intact and cracked backfill

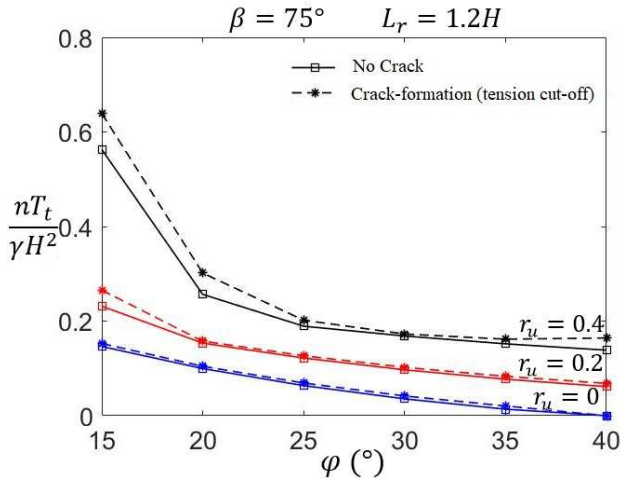
350

351 The soil friction influence on the tensile strength of the geosynthetic reinforcements used to maintain the reinforced  
 352 soil wall stability is presented in Fig. 7 for different pore pressure coefficients. An uniform backfill soil and a horizontal  
 353 seismic coefficient equal to 0.1 are considered. It is clear that higher friction angle implies better quality backfills and  
 354 therefore, that the required reinforcement strength is higher in case lower friction angle values for both reinforced soil  
 355 structures inclinations and different values of  $r_u$ , considering or not the presence of cracks. The effect of the soil friction  
 356 angle  $\varphi$  increases with the increases of the values of  $r_u$ . The required reinforcement strength is slightly greater for the  
 357 crack presence case. It is important to note that this difference between the results obtained considering or not the crack  
 358 presence decreases when increasing the soil friction angle  $\varphi$  as well as when decreasing the pore-water coefficient  $r_u$   
 359 and the wall inclination.

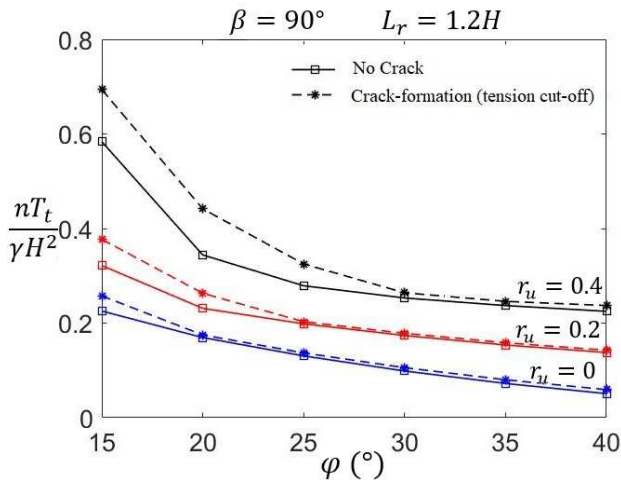
360 For the inclined retaining wall with  $\beta = 75^\circ$ , the required reinforcement strength that assure the reinforced soil wall  
 361 stability is equal to zero for a soil friction angle higher than  $37^\circ$  and a zero pore-water coefficient  $r_u$  value.

362





363



364

365

366

**Fig. 7.** Required reinforcement strength against soil friction angle for intact and cracked backfill

367

7.2 Required reinforcement strength for reinforced non-homogeneous soil retaining walls

368

Most previous studies on the reinforced soil retaining walls stability assume a homogeneous soil. However, soils are non-homogeneous in nature and their properties show spatial variability (Pan and Dias, 2015). This heterogeneity affects the reinforced soil retaining walls stability, hence the importance of its consideration in the design. The conventional kinematic theorem can only be used in cases of homogeneous soils. The discretization-based kinematic analysis method gives the ability to overcome this limitation, and to consider the soil heterogeneity. The variation of the soil strength parameters, the soil friction angle and cohesion, are considered. On the other hand, the soil unit weight  $\gamma$  is considered constant in the whole domain. In this study, for convenience and simplicity, two types of heterogeneity are considered: the soil properties increase linearly with depth and layered backfill soil profile.

376

7.2.1 Linearly increased soil strength profile

377

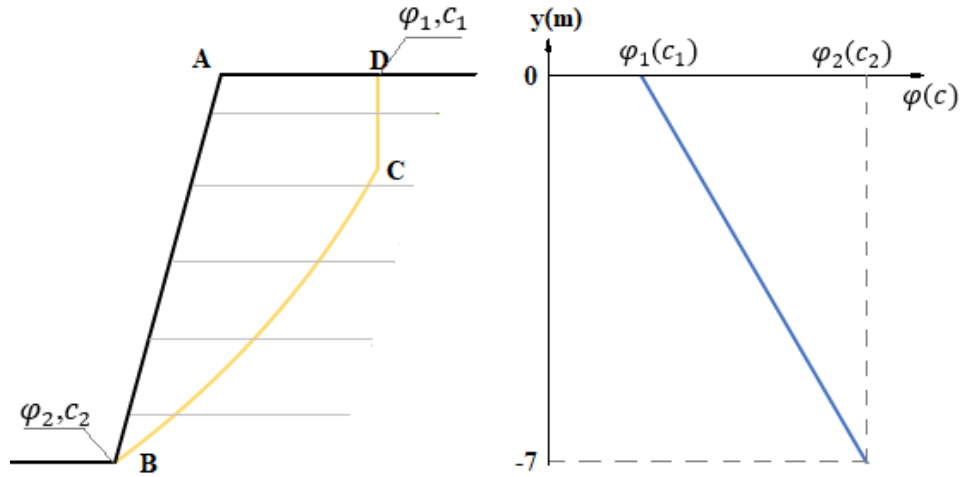
The soil strength parameters are assumed to vary linearly only in the vertical direction (Fig. 8). This means that they are assumed to be constant in the horizontal plane, i.e. at the same depth. The soil unit weight variation is neglected in

378

379 the whole domain.  $c_1$  and  $\varphi_1$  are respectively the soil cohesion and friction angle at the ground surface, while  $c_2$  and  
 380  $\varphi_2$  are those at the wall toe level.

381

382



383

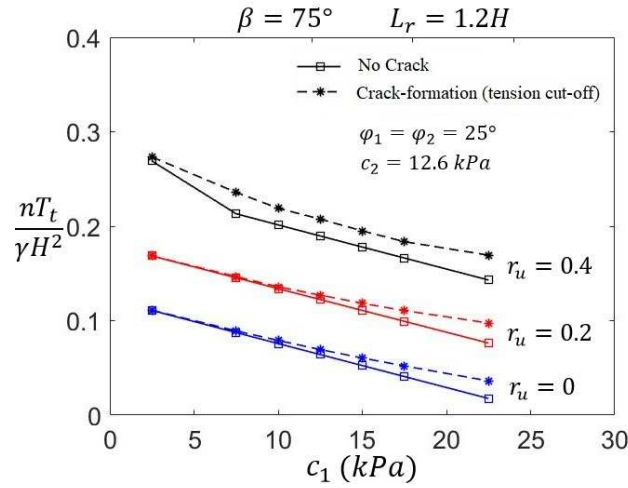
384

**Fig.8.** Distribution of the soil properties with depth

385 The effect of each soil strength parameters variability is investigated separately. When analyzing the influence of a  
 386 parameter, the second one is taken as constant. An inclined reinforced earth wall with  $\beta=75^\circ$  is considered. The other  
 387 parameters are kept the same as the previous section:  $H=7\text{ m}$ ,  $\gamma=18\text{ kN/m}^3$ ,  $\delta\theta=0.01^\circ$ ,  $k_h=0.1$ ,  $\lambda=0.5$ ,  $L_r=1.2\text{ H}$ ,  
 388  $n=10$ ,  $f_0^*=1.2$ ,  $f_1^*=0.6$ ,  $f=1.2$ ,  $V_s=150\text{ m/s}$ ,  $V_p=280.5\text{ m/s}$ , and  $T=0.3\text{ s}$

389 First, the influence of the soil cohesion variability is investigated. The required normalized reinforcement strength is  
 390 plotted against different ground surface soil cohesion values  $c_1$  (Fig. 9). The soil cohesion at the wall toe level is kept  
 391 equal to  $c_2=12.6\text{ kPa}$ . The soil friction angle is considered constant across the whole field  $\varphi_1=\varphi_2=25^\circ$ .

392 A decrease of the required reinforcement strength is observed when  $c_1$  increases from 2.5 to 22.5 kPa for both  
 393 cases of intact or cracked soil. The required reinforcement strength obtained in case of crack formation is higher than  
 394 the case of an intact soil. The difference between the two cases is more pronounced for greater values of  $c_1$ . The  
 395 required reinforcement strength decreases linearly with  $c_1$  for the case of water-pressure coefficients  $r_u$  equals to 0 and  
 396 0.2. However, for  $r_u = 0.4$ , the rate of decrease is greater for  $c_1$  smaller than 7.5 kPa. This can be explained by the  
 397 reinforcements pullout failure that occurs in some layers under these conditions.



398

399

**Fig. 9.** Required reinforcement strength against non-uniform soil cohesion for intact and cracked backfill

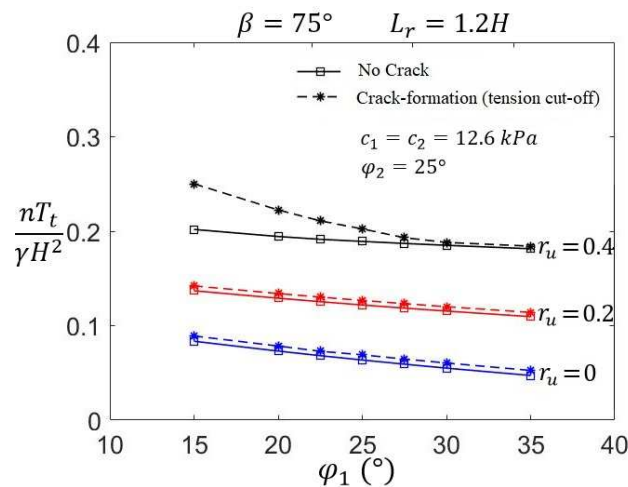
400

The influence of the soil friction angle variability is also investigated apart. The required normalized reinforcement strength is plotted against different ground surface soil friction angles  $\varphi_1$  (Fig. 10). The soil friction angle at the wall toe level is kept equal to  $\varphi_2=25^\circ$ . The soil cohesion is considered constant across the whole field  $c_1=c_2=12.6\text{ kPa}$ .

403

The increase of  $\varphi_1$  from  $15^\circ$  to  $35^\circ$  decreases slightly the required normalized reinforcement strength and therefore, this increase slightly enhances the reinforced earth wall stability for both intact and cracked soils and different values of  $r_u$ . The required reinforcement strength is slightly greater for the crack presence case except the case of pore-water pressure  $r_u$  equal to 0.4, and precisely for soil friction angle  $\varphi_1$  at the wall toe smaller than  $25^\circ$ . Wherein that case, the difference between the intact soil case and the cracked soil one becomes significant, and increases with the soil friction angle  $\varphi_1$  decrease. This is because the reinforcements pullout failure in some layers in the case of cracked soils.

409



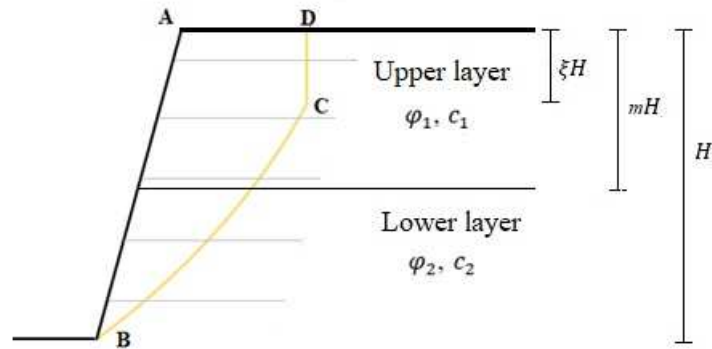
410

411

**Fig. 10.** Required reinforcement strength against non-uniform soil friction angle for intact and cracked backfill

412 7.2.2 Layered soil profile

413 In most of the real cases, the soil profile is a layered one. In this section, a reinforced soil retaining wall with a  
414 stratified backfill composed of two soil layers with different soil strength parameters (see Fig. 11), is analyzed using the  
415 developed method. A coefficient  $m$  is defined to distinguish the stratified condition as the ratio of the upper layer height  
416 to the wall height. The soil strength parameters are  $\varphi_1$  and  $c_1$  in the upper layer and  $\varphi_2$  and  $c_2$  in the lower one.

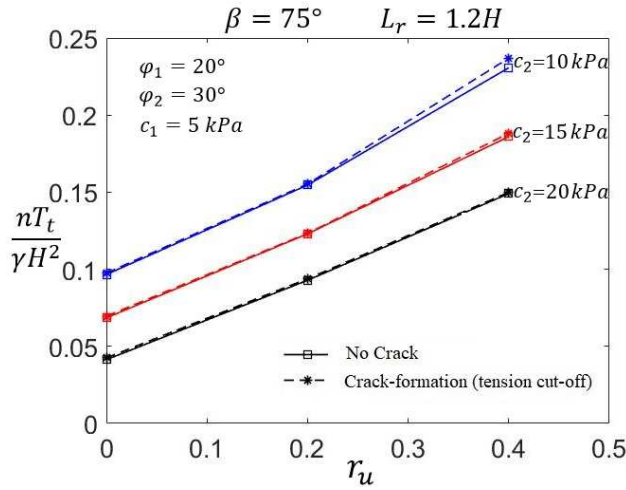


417  
418 **Fig. 11.** Heterogeneous backfill with two soil layers

419 The reinforced soil wall considered is inclined with  $\beta=75^\circ$  and all the parameters are kept the same as the previous  
420 sections except the soil strength parameters. Fig. 12 shows the pore-water pressure coefficient  $r_u$  and soil cohesion  $c_2$  of  
421 the lower layer influences on the normalized required reinforcement strength. The analysis without the presence of  
422 cracks as well as the case of crack formation are both considered. A two-layered backfill required higher reinforcement  
423 strength in order to prevent the structure failure when the coefficient  $r_u$  increased and when the soil cohesion  $c_2$  in the  
424 lower layer decreased.

425 The required reinforcement strength is slightly greater in case of the crack presence in the failure surface. An  
426 increase in the lower layer soil cohesion  $c_2$  from 10 to 20 kPa leads to 35.37% and 36.73% reduction of the  
427 normalized required reinforcement strength for intact and cracked soil respectively, for a pore-water pressure  
428 coefficient equal to 0.4. These reductions become respectively equal to 57.21% and 56.35% for intact and cracked  
429 soils when the pore-water pressure does not exist ( $r_u = 0$ ).

430



431

432

**Fig. 12.** Required reinforcement strength against  $r_u$  and soil cohesion  $c_2$  for a two-layered backfill

433

434

435

436

437

Fig. 13 illustrates the influence of the pore-water pressure coefficient  $r_u$  and lower layer soil friction angle  $\varphi_2$  on the normalized required reinforcement strength. The same two crack cases are considered. The stability of the reinforced soil wall is improved when the coefficient  $r_u$  decreased and when the soil friction angle  $\varphi_2$  in the lower layer increased. This is logical since the water has a destabilizing effect and the soil friction angle increase enhances the wall stability by providing an additional resistance.

438

439

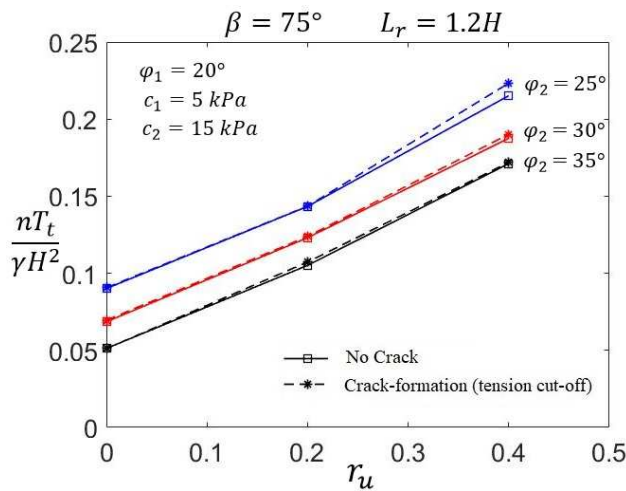
440

441

442

Considering the crack formation through the failure mechanism leads to a higher required reinforcement strength. A decrease in the lower layer soil friction angle  $\varphi_2$  from 35 to 25° leads to respectively 75.8% and 77.12% of normalized required reinforcement strength increase for intact and cracked soil, for a zero pore-water pressure coefficient. These increases become respectively equal to 25.73% and 29.84% for intact and cracked soil when the pore-water pressure coefficient is equal to 0.4.

443



444

445

**Fig. 13.** Required reinforcement strength against  $r_u$  and soil friction angle  $\varphi_2$  for a two-layered backfill

## 446 8 Conclusion

447 This paper investigates the seismic internal stability of geosynthetic reinforced saturated soil wall considering soil  
448 cracks, using the kinematic theorem of limit analysis combined with the discretization technique. The results are  
449 presented in terms of required reinforcement strength that prevent wall failure. The discretization technique consists to  
450 generate the rotational sliding surface of the reinforced soil wall point by point based on the associated flow rule. This  
451 method represents a suitable tool to overcome the limitations of the conventional upper bound limit analysis method. It  
452 gives the ability to easily integrate the soil spatial variability properties for nonhomogeneous or multi-layered soils. In  
453 addition of the benefits of considering the soil heterogeneity, it allows the implementation of the pseudo-dynamic  
454 approach which takes into account the aspects neglected by the pseudo-static approach adopted in the conventional  
455 kinematic analysis. The effect of the buoyancy forces and seepage forces are considered. It is included as an additional  
456 external force in the limit analysis upper bound method.

457 In order to validate the proposed approach, the obtained results are verified by comparison with those obtained by  
458 Abd and Utili (2017), who evaluated the reinforced slopes stability, using the conventional upper bound approach of  
459 limit analysis. Pre-existing crack as well as crack formation through the collapse mechanism are considered without  
460 consideration of the seismic loading. A good consistency between the two approaches proves the developed method  
461 effectiveness.

462 The effects of the crack presence, seismic loading and the soil strength parameters on the required reinforcement  
463 strengths are assessed. Three scenarios are considered for the backfill soil strength parameters, a homogeneous soil,  
464 non-homogeneous soil with a linearly increased strength parameters or a layered backfill.

465 The consideration of the crack formation is found to have a destabilizing effect on the reinforced soil retaining walls  
466 stability. This is more pronounced for lower soil friction angle values, greater values of soil cohesion and pore water  
467 coefficient.

468 The pore water pressure has also a negative effect on these structures. In addition, the required reinforcement  
469 strength is highly dependent on the soil strength parameters. The soil friction angle and cohesion enhance the reinforced  
470 soil wall stability.

471 The discretization-based kinematic analysis have shown its effectiveness for the seismic internal stability analysis of  
472 reinforced saturated soil retaining walls with crack presence. The key advantage of this method is its capacity to deal  
473 with multi-layered or nonhomogeneous soil profiles. In addition, it allows the implementation of the pseudo-dynamic  
474 approach which gives the benefits of considering the dynamic characteristic of the seismic loading.

475 **Numerical calculations or physical models will be necessary to evaluate the reliability of the developed method in**  
476 **this paper.**

477 **References**

- 478 Abd, A.H., Utili, S., 2017. Design of geosynthetic-reinforced slopes in cohesive backfills. *Geotext. Geomembranes* 45,  
479 627–641. <https://doi.org/10.1016/j.geotexmem.2017.08.004>
- 480 Ahmad, S.M., Choudhury, D., 2008. Pseudo-dynamic approach of seismic design for waterfront reinforced soil-wall.  
481 *Geotext. Geomembranes* 26, 291–301. <https://doi.org/10.1016/j.geotexmem.2007.12.004>
- 482 Alhadj Chehade, H., Dias, D., Sadek, M., Jenck, O., Hage Chehade, F., 2021. Pseudo-static Analysis of Reinforced  
483 Earth Retaining Walls. *Acta Geotech.* 2. <https://doi.org/10.1007/s11440-021-01148-2>
- 484 Alhadj Chehade, H., Dias, D., Sadek, M., Jenck, O., Hage Chehade, F., 2020. Upper bound seismic limit analysis of  
485 geosynthetic-reinforced unsaturated soil walls. *Geotext. Geomembranes*.  
486 <https://doi.org/10.1016/j.geotexmem.2020.02.001>
- 487 Alhadj Chehade, H., Dias, D., Sadek, M., Jenck, O., Hage Chehade, F., 2019. Seismic analysis of geosynthetic-  
488 reinforced retaining wall in cohesive soils. *Geotext. Geomembranes* 47, 315–326.  
489 <https://doi.org/10.1016/j.geotexmem.2019.02.003>
- 490 Baker, R., 1981. Tensile strength, tension cracks, and stability of slopes. *Soils Found.* 21, 1–17.  
491 [https://doi.org/10.3208/sandf1972.21.2\\_1](https://doi.org/10.3208/sandf1972.21.2_1)
- 492 Baker, R., Leshchinsky, D., 2003. Spatial distribution of safety factors: Cohesive vertical cut. *Int. J. Numer. Anal.*  
493 *Methods Geomech.* 27, 1057–1078. <https://doi.org/10.1002/nag.312>
- 494 Baker, R., Leshchinsky, D., 2001. Spatial distribution of safety factors. *J. Geotech. Geoenvironmental Eng.* 127, 135–  
495 145. [https://doi.org/10.1061/\(ASCE\)1090-0241\(2001\)127:2\(135\)](https://doi.org/10.1061/(ASCE)1090-0241(2001)127:2(135))
- 496 Basha, B.M., Sivakumar Babu, G.L., 2011. Seismic reliability assessment of internal stability of reinforced soil walls  
497 using the pseudo-dynamic method. *Geosynth. Int.* 18, 221–241. <https://doi.org/10.1680/gein.2011.18.5.221>
- 498 Chen, W.-F., Giger, M.W., Fang, H.Y., 1969. On the limit analysis of stability of slopes. *Soils Found.* 9, 23–32.  
499 [https://doi.org/10.3208/sandf1960.9.4\\_23](https://doi.org/10.3208/sandf1960.9.4_23)
- 500 Choudhury, D., Nimbalkar, S.S., 2006. Pseudo-dynamic approach of seismic active earth pressure behind retaining  
501 wall. *Geotech. Geol. Eng.* 24, 1103–1113. <https://doi.org/10.1007/s10706-005-1134-x>
- 502 Chowdhury, R.N., Zhang, S., 1991. Tension cracks and slope failure, in: *Proceedings of the International Conference:*  
503 *Slope Stability Engineering, Developments and Applications.* Thomas Telford, London, pp. 27–32.  
504 <https://doi.org/10.1680/ssedaa.16606.0005>
- 505 Guler, E., Hamderi, M., Demirkan, M.M., 2007. Numerical analysis of reinforced soil-retaining wall structures with  
506 cohesive and granular backfills. *Geosynth. Int.* 14, 330–345. <https://doi.org/10.1680/gein.2007.14.6.330>
- 507 Guo, X., Dias, D., Carvajal, C., Peyras, L., Breul, P., 2018. Reliability analysis of embankment dam sliding stability

508 using the sparse polynomial chaos expansion. *Eng. Struct.* 174, 295–307.

509 <https://doi.org/10.1016/j.engstruct.2018.07.053>

510 Hu, Y., Zhang, G., Zhang, J.-M., Lee, C.F., 2010. Centrifuge modeling of geotextile-reinforced cohesive slopes.

511 *Geotext. Geomembranes* 28, 12–22. <https://doi.org/10.1016/j.geotexmem.2009.09.001>

512 Koerner, R.M., Koerner, G.R., 2018. An extended data base and recommendations regarding 320 failed geosynthetic

513 reinforced mechanically stabilized earth (MSE) walls. *Geotext. Geomembranes* 46, 904–912.

514 <https://doi.org/10.1016/j.geotexmem.2018.07.013>

515 Ling, H.I., Leshchinsky, D., Chou, N.S., 2001. Post-earthquake investigation on several geosynthetic-reinforced soil

516 retaining walls and slopes during the ji-ji earthquake of Taiwan. *Soil Dyn. Earthq. Eng.* 21, 297–313.

517 [https://doi.org/10.1016/S0267-7261\(01\)00011-2](https://doi.org/10.1016/S0267-7261(01)00011-2)

518 Michalowski, R.L., 2013. Stability assessment of slopes with cracks using limit analysis. *Can. Geotech. J.* 50, 1011–

519 1021. <https://doi.org/10.1139/cgj-2012-0448>.

520 Mollon, G., Dias, D., Soubra, A.-H., 2011. Rotational failure mechanisms for the face stability analysis of tunnels

521 driven by a pressurized shield. *Int. J. Numer. Anal. Methods Geomech.* 35, 1363–1388.

522 Nimbalkar, S.S., Choudhury, D., Mandal, J.N., 2006. Seismic stability of reinforced-soil wall by pseudo-dynamic

523 method. *Geosynth. Int.* 13, 111–119. <https://doi.org/10.1680/gein.2006.13.3.111>

524 Pan, Q., Dias, D., 2015. Face Stability Analysis for a Shield-Driven Tunnel in Anisotropic and Nonhomogeneous Soils

525 by the Kinematical Approach. *Int. J. Geomech.* 16, 04015076. [https://doi.org/10.1061/\(ASCE\)GM.1943-](https://doi.org/10.1061/(ASCE)GM.1943-5622.0000569)

526 [5622.0000569](https://doi.org/10.1061/(ASCE)GM.1943-5622.0000569)

527 Porbaha, A., Goodings, D., 1996. Centrifuge modeling of geotextile-reinforced cohesive soil retaining walls. *J.*

528 *Geotech. Eng.* 122, 840–848. [https://doi.org/10.1061/\(ASCE\)0733-9410\(1996\)122:10\(840\)](https://doi.org/10.1061/(ASCE)0733-9410(1996)122:10(840))

529 Qin, C.-B., Chian, S.C., 2019. Pseudo-static/dynamic solutions of required reinforcement force for steep slopes using

530 discretization-based kinematic analysis. *J. Rock Mech. Geotech. Eng.* 11, 289–299.

531 <https://doi.org/10.1016/j.jrmge.2018.10.002>

532 Qin, C.-B., Chian, S.C., 2018. Bearing capacity analysis of a saturated non-uniform soil slope with discretization-based

533 kinematic analysis. *Comput. Geotech.* 96, 246–257. <https://doi.org/10.1016/j.compgeo.2017.11.003>

534 Qin, C.-B., Chian, S.C., 2017. Kinematic analysis of seismic slope stability with a discretisation technique and pseudo-

535 dynamic approach: a new perspective. *Géotechnique* 68, 492–503. <https://doi.org/10.1680/jgeot.16.P.200>

536 Riccio, M., Ehrlich, M., Dias, D., 2014. Field monitoring and analyses of the response of a block-faced geogrid wall

537 using fine-grained tropical soils. *Geotext. Geomembranes* 42, 127–138.

538 <https://doi.org/10.1016/j.geotexmem.2014.01.006>

539 Steedman, R.S., Zeng, X., 1990. The influence of phase on the calculation of pseudo-static earth pressure on a retaining



540 wall. *Géotechnique* 40, 103–112. <https://doi.org/10.1680/geot.1990.40.1.103>

541 Sun, Z., Li, J., Pan, Q., Dias, D., Li, S., Hou, C., 2018. Discrete Kinematic Mechanism for Nonhomogeneous Slopes  
542 and Its Application. *Int. J. Geomech.* 18, 04018171. [https://doi.org/10.1061/\(asce\)gm.1943-5622.0001303](https://doi.org/10.1061/(asce)gm.1943-5622.0001303)

543 Utili, S., 2013. Investigation by limit analysis on the stability of slopes with cracks. *Géotechnique* 63, 140–154.  
544 <https://doi.org/10.1680/geot.11.P.068>

545 Utili, S., Abd, A.H., 2016. On the stability of fissured slopes subject to seismic action. *Int. J. Numer. Anal. Methods*  
546 *Geomech.* 40, 785–806. <https://doi.org/10.1002/nag.2498>

547 Viratjandr, C., Michalowski, R.L., 2006. Limit analysis of submerged slopes subjected to water drawdown. *Can.*  
548 *Geotech. J.* 43, 802–814. <https://doi.org/10.1139/T06-042>

549 Zhao, L.H., Cheng, X., Zhang, Y., Li, L., Li, D.J., 2016. Stability analysis of seismic slopes with cracks. *Comput.*  
550 *Geotech.* 77, 77–90. <https://doi.org/10.1016/j.compgeo.2016.04.007>

551

552